Elastic FWI for joint Vp, Vs and density inversion

Peng Shen, Uwe Albertin, Hermes Malcotti, Josh Haataja, Chevron Technical Center, a division of Chevron U.S.A. Inc.

SUMMARY

We apply a Vp−Vs−density parametrization in elastic FWI to invert hydrophone seismic data for these subsurface earth properties. Inversion of these parameters from hydrophone seismic data is possible due to the AVA behavior of this data, which is directly related to elastic parameter contrasts across subsurface interfaces. A natural framework to implement such an inversion is elastic FWI, and in order to accomplish this, we utilize an adjoint-state approach that computes objective-function gradients suitable for joint simultaneous elastic inversion for Vp, Vs and density without any reference to well-log constraints. Eliminating the use of well-log constraints is one of our main objectives, since it potentially offers a significant advantage over standard AVA analysis derived from migrated image gathers which often relies on such constraints to obtain an accurate inversion. Inverted acoustic impedance, density, and vp-vs ratios from our elastic FWI compare well with well-logs and standard AVA results obtained from migrated gathers, suggesting that elastic FWI is robust for the determination of elastic subsurface earth properties directly from hydrophone data.

INTRODUCTION

Earth properties such as Vp, Vs and density influence seismic data through different mechanisms. Conventionally we associate traveltime with Vp, the p-wave velocity, for its leading-order sensitivity to kinematics. Acoustic FWI techniques used in production today often rely on kinematic time-shifts in the formulation of the residual used when recovering Vp; use of such time-shifts mitigates the effects of amplitude differences between acoustic forward-modelled data and the elastic effects present in field data. However, this mitigation typically precludes these methods from recovering elastic parameters Vs and density.

As a result, there has been significant recent interest to extend FWI elastically. Extension of FWI from acoustic to elastic (Borisov and Singh, 2015; Solano and Plessix, 2023; Operto et al., 2023) not only honors the physics of wave propagation through the medium, it also distinguishes itself from acoustic FWI in the accurate modeling of reflection behavior at subsurface interfaces. Depending on what elastic-parameter contrasts are present across an interface, acoustic modeling of p-wave data using a Vp contrast alone will often be unable to explain seismic reflection amplitudes and phases across the full reflection angle range, even when the velocity is correct. This inability actually forms a critical underlying principle in standard AVO analysis, that is that the elastic amplitude and phase changes as a function of angle remain in migrated reflectivity gathers after migration. They are not removed by the acoustic modeling and Kirchhoff-reflectivity imaging condition in a typical migration algorithm, hence enabling a post-migration recovery of elastic parameters from the gathers.

In contrast, an elastic FWI that uses only hydrophone data relies on the angle-dependent behavior of the amplitudes and phases in the data to produce an elastic signature in the FWI residual, such as a least-squares residual, which occurs if the elastic model is not correct. Standard adjoint-based backprojection can then, in principle, recover the elastic coefficients until the modeled hydrophone data matches the field data. The Heaviside singularities recovered in this way may be viewed as the leading order influencers to the amplitude and phase variations in angle. One might expect that the accuracy and separability of elastic parameters in an elastic FWI based on hydrophone data might be similar to that of standard AVO inversion after migration in media that are relatively simple and stratified. However, the nonlinear nature of an FWI inversion, with its improved ability to recover Heaviside-type singularities, together with appropriate parametrizations that improve parameter separation, suggests that elastic FWI may actually perform significantly better than standard AVO, particularly in areas where little well control is present.

This work continues from our previous sequence of works, Albertin et al. (2016), Shen and Albertin (2017), Shen et al. (2018), Shen et al. (2020), describing our method for a joint elastic full waveform inversion of Vp, Vs, and density. We first summarize the theoretical basis of our method, and then proceed to show a field-data example of p-impedance, Vp/Vs ratio, and density recovery from elastic FWI without using well control. We then illustrate how well our method performs relative to a standard AVO analysis relying on typical well control performed after migration.

METHOD

The elastic wave equation can be written as

$$\partial_t \begin{pmatrix} \mathbf{v} \\ \boldsymbol{\sigma} \end{pmatrix} = \begin{pmatrix} b & 0 \\ 0 & C \end{pmatrix} \begin{pmatrix} 0 & \nabla_h \\ \nabla_v & 0 \end{pmatrix} \begin{pmatrix} \mathbf{v} \\ \boldsymbol{\sigma} \end{pmatrix} + \begin{pmatrix} 0 \\ f \end{pmatrix}. \quad (1)$$

Here $b = \frac{1}{\rho}$ is the buoyancy and ρ is the density, $\mathbf{v}$ is the particle velocity, $\boldsymbol{\sigma}$ is stress in the Voigt notation, C is matrix of the reduced stiffness tensor, f is the pressure source field, and $\nabla_h = \begin{pmatrix} \nabla_d & \nabla_s \end{pmatrix}$, $\nabla_v = \begin{pmatrix} \nabla_d \\ \nabla_s \end{pmatrix}$, where

$$\nabla_d = \begin{pmatrix} \partial_1 & 0 & 0 \\ 0 & \partial_2 & 0 \\ 0 & 0 & \partial_3 \end{pmatrix},$$

$$\nabla_s = \begin{pmatrix} 0 & \partial_3 & \partial_2 \\ \partial_3 & 0 & \partial_1 \\ \partial_2 & \partial_1 & 0 \end{pmatrix}.$$

We set the objective function to be

$$J = \frac{1}{2}||S\boldsymbol{\sigma} - \mathbf{d}^{\mathbf{obs}}||^2 - \frac{\alpha}{2}||\mathbf{d}^{\mathbf{obs}} \circ S\boldsymbol{\sigma}||^2. \quad (2)$$

Here S is a sampling operator, $\mathbf{d^{obs}}$ is the observed data, $||\cdot||$ is an L_2 norm, $\circ$ indicates correlation, and α is a small positive real number. The stack-power term represented as the correlation is used to regulate the data residual. Let $*$ be convolution operator, the residual wavefield becomes

$$R = S^*(S\sigma - \mathbf{d^{obs}}) - \alpha S^* \mathbf{d^{obs}} * (\mathbf{d^{obs}} \circ S\sigma)). \quad (3)$$

Let $\mathbf{u}$ be the adjoint-state particle velocity, τ be the adjoint-state stress under the Voigt notation, and ∂_t^* be the time partial derivative in reverse-time, the adjoint-state wavefield satisfies

$$\partial_t^* \begin{pmatrix} \mathbf{u} \\ \tau \end{pmatrix} = - \begin{pmatrix} 0 & \nabla_h \\ \nabla_v & 0 \end{pmatrix} \begin{pmatrix} b & 0 \\ 0 & C \end{pmatrix} \begin{pmatrix} \mathbf{u} \\ \tau \end{pmatrix} + \begin{pmatrix} 0 \\ R \end{pmatrix} \quad (4)$$

The apparent gradient for ρ and the C_{ij} of the stiffness matrix are collected as

$$\frac{\partial J}{\partial b} = \int dt \sigma_{ij} u_j \quad (5)$$

$$\frac{\partial J}{\partial C_{ij}} = \int dt (Dv_i \tau_j + Dv_j \tau_i)/(1+\delta_{ij}) \quad (6)$$

The summation convention for repeated indices is implied in equation (5), and in the sequel. In equation (6), δ_{ij} is the Kronecker delta, and Dv is defined as

$$Dv_1 = v_{1,1} \quad (7)$$

$$Dv_2 = v_{2,2} \quad (8)$$

$$Dv_3 = v_{3,3} \quad (9)$$

$$Dv_4 = v_{2,3} + v_{3,2} \quad (10)$$

$$Dv_5 = v_{1,3} + v_{3,1} \quad (11)$$

$$Dv_6 = v_{1,2} + v_{2,1} \quad (12)$$

By the chain rule, the gradient to density, ρ, can be written as

$$\frac{\partial J}{\partial \rho} = -\frac{1}{\rho^2}\frac{\partial J}{\partial b} + \frac{\partial J}{\partial C_{ij}}\frac{\partial C_{ij}}{\partial \rho} \quad (13)$$

The gradient to V_p and V_s are obtained via chain rule as

$$\frac{\partial J}{\partial V_p} = \frac{\partial J}{\partial C_{ij}}\frac{\partial C_{ij}}{\partial V_p} \quad (14)$$

$$\frac{\partial J}{\partial V_s} = \frac{\partial J}{\partial C_{ij}}\frac{\partial C_{ij}}{\partial V_s} \quad (15)$$

The objective function of equation (2) and the gradients in ρ, V_p, V_s, as represented by equations (13), (14), (15), respectively, are employed to build the elastic FWI iterative scheme.

EXAMPLE

We apply the method described above to a hydrophone dataset. The initial Vp velocity model, as shown in Fig.(1a), is devoid of structures of large wavenumber. The initial density model is derived according to the Gardner relation based on the initial Vp model. The water density is set to unity. The initial Vs model is derived according to $V_s = V_p/1.7$ in the sediment, and $V_s = 0$ in the water. A bootstrapping frequency scheme is used to raise the frequency band gradually from an initial peak frequency of 7Hz to a final peak frequency of 25Hz, with the final amplitude being 20 dB down from peak at 30Hz.

We compare our results against a standard geo-statistical inversion. The high frequency character of the geo-statistical inversion comes from the utilization of a production high frequency ($\geq$70Hz) Kirchhoff image together with gathers and well-log constraints. It's worth noting that the elastic FWI does not use any well information. The statistical inversion was conducted to derive Vp, Vs, VpVs ratio, and density, which are currently considered as the best knowledge we have for the earth parameters in the area of investigation. In Fig.(1c) we compare at reservoir scale the geo-statistical inverted Vp (Fig.1b) and the inverted Vp from elastic FWI. The Vp model from elastic FWI captures faults and major events which are in good one-to-one agreement with the geo-statistical Vp, despite the FWI being run to lower frequency. From left to right, Fig.(1d) shows the Vp-log, Vs-log, density-log, VpVs-ratio-log and the acoustic impedance log, overlaid with initial and final depth profiles extracted from the corresponding parameters in the elastic FWI model. The magenta, blue and the black are, respectively, the initial and final results from elastic FWI, and a well log, wavenumber-filtered to match the FWI spectrum. In general, there is close agreement with well-log data when comparing with elastic FWI results.

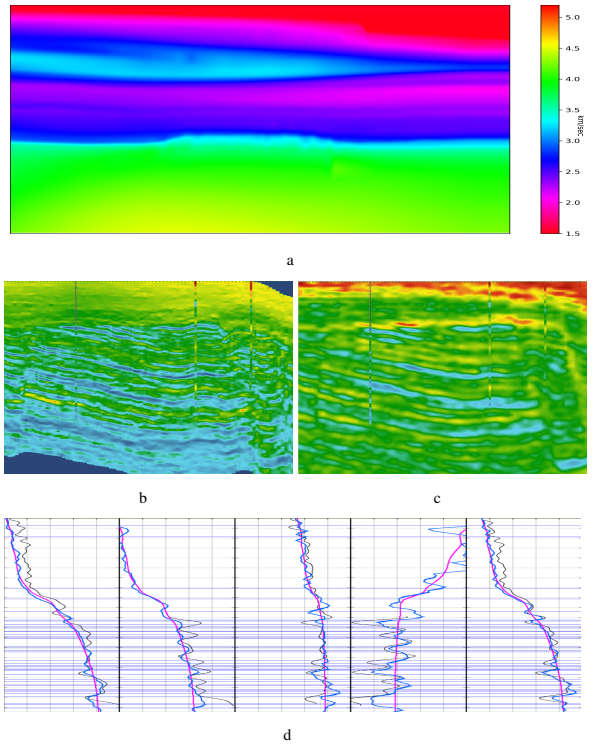

Figure 1: Initial velocity and reservoir scale comparison with the geo-statistical inversion and well-log. (a) Initial Vp model. (b) Geo-statistical inverted V_p model based on a Kirchhoff image of approximately 70Hz. (c) Elastic FWI inverted V_p model shown at the same reservoir scale. (d) Well-log comparison. Panels from left to right are 1) Vp, 2) Vs, 3) density, 4) VpVs ratio, and 5) acoustic impedance. The magenta, blue and black cures are initial depth profile, elastic FWI inverted and filtered log, respectively.

Although density results from the geo-statistical inversion proved to be unreliable, a rough qualitative estimate of density can be obtained from conventional imaging from the far offset stack, as it tends to negatively correlate with density variations. High far offset stack amplitudes are associated with low density and vice-versa. Figure (2a) compares the far offset stack amplitude and the density inversion depth slice from elastic FWI. Blue color corresponds to low values while red and magenta correspond to high. In comparing the two images, it is clear that they negatively correlate on a long-wavelength scale, with blues in the far-offset amplitude plot correlating well with red and magenta in the FWI density, particularly on the left side of the section.

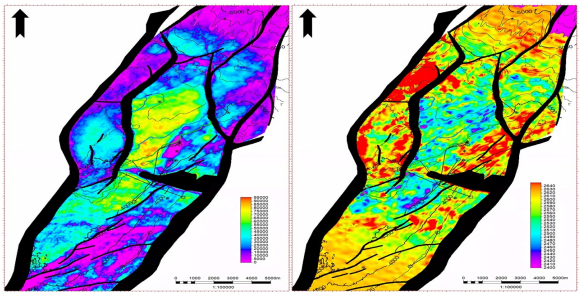

a

Figure 2: Comparison of far offset stack and the inverted density from elastic FWI in depth slice. Left: far offset stack; right: elastic FWI inverted density depth slice.

To examine density at the reservoir scale, we show the inverted density in Fig.3a overlaid with density well-logs. We observe that the location and amplitude of density variations correlate well with the density log despite the well log having higher resolution. As Shown in Figure (3b), the signature on the well-log plot associated with a high quality sand (of extra low density) coincides with the low-density anomaly from inverted FWI density. This density result suggests that elastic FWI is effective in recovering band-limited density directly from surface seismic data, without any well-log data or constraint being used.

Hydrocarbon indicators are usually tied to sands which typically have low density values. Rock physics predicts that high-quality sands are also associated with high values of Vs and low values of Vp. To be sure that the elastic FWI is not accidentally producing low density values at locations of high quality sands, we make facies plots of sands overlaid with depth profiles extracted from inverted Vs and Vp. Shown in Fig.(3c), the depth profiles extracted from the inverted density model and the Vs model are plotted in magenta and in green, respectively. Their initial depth profiles before inversion are recorded as smooth curves in blue. The shear velocities are high at the cyan facies characterized by the high quality sands. A similar overlay of facies of sand and Vp are shown in Fig.(3d), where, again, the depth profile of the inverted density is plotted in magenta, but the inverted Vp is plotted in red, and their initial depth profiles are depicted as smooth curves in blue. The cyan-colored high quality sands coincide with low Vp values. The parity comparison between

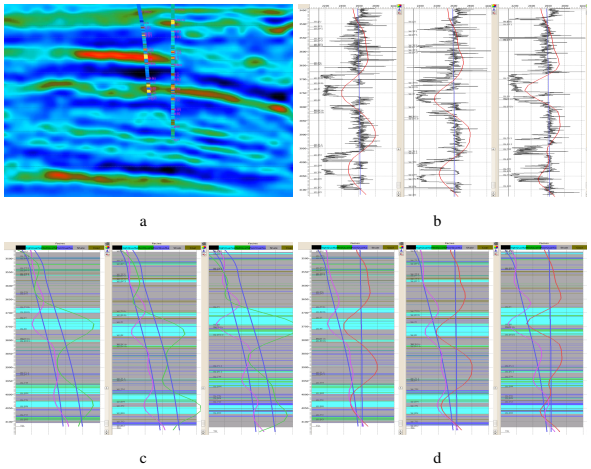

a b c d

Figure 3: (a) Reservoir scale inverted density model overlaid with density well-log. (b) Depth profiles extracted from inverted density model overlaid with density log from selected wells. (c) EFWI inverted low density and high Vs coincide with high quality sand. Facies plot of concentration of high quality sand overlaid with the depth profiles extracted from density model and Vs model. Magenta: output density, green: output Vs, the initial density and Vs are plotted in blue. (d) EFWI inverted low density and low Vp coincide with high quality sand. Facies plot of concentration of high quality sand overlaid with the depth profiles extracted from density model and Vp model. Magenta: output density, red: output Vp, the initial density and Vp are plotted in blue.

Fig.(3c) and Fig.(3d) clearly demonstrates the correspondence with high quality sands, low density, low Vp but high Vs, a unique material attribute combination that completely agrees with the prediction of rock physics. This confirms that the sensitivity in Vp, Vs, and density to elastic reflection parameters is sufficient to inversely determine these parameters from surface acquired reflection data.

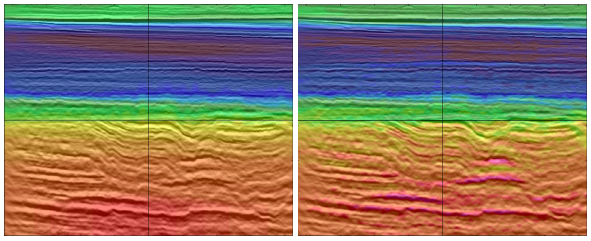

a b

Figure 4: (a) Initial density model overlaid with the initial seismic image obtained from migration using initial Vp. (b) Output density model from elastic FWI overlaid with the final seismic image obtained from migration using the final Vp model from elastic FWI.

We close the FWI density examination by showing the overlaid seismic image and density. The initial image overlaid with the initial density model is shown in Fig.(4a). No other addi-

tional information for density recovery in the FWI was provided. Figure (4b) shows the final seismic image overlaid with the final density model. The final seismic image is migrated using the final Vp model from the elastic FWI. The prospect area is well correlated with the output density model by the low amplitude anomalies. At the same time, the geometric definition of the prospect is also slightly sharper in the FWI result.

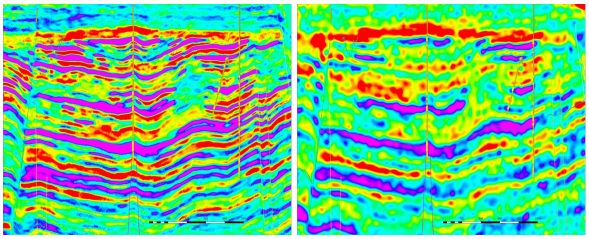

a b

Figure 5: (a) Geo-statistical VpVs ratio based on Kirchhoff image of 70Hz. (b) VpVs ratio obtained by dividing the output Vp model by the output Vs model from elastic FWI.

The reservoir-scale parity comparison of the geo-statistical inversion of VpVs ratio and the VpVs ratio obtained from dividing the Vp model by the Vs model from elastic FWI is shown in Figure (5). Figure (5a) is the statistically derived VpVs ratio based on a Kirchhoff image at 70Hz with utilization of well information, which is considered by us the best knowledge of the VpVs ratio of the studied area. The VpVs ratio obtained by taking the ratio of output Vp model and the Vs model from elastic FWI is shown in Figure (5b). The correspondence between Fig.(5a) and Fig.(5b) is clear not only in event positioning but also in amplitude. One area where elastic FWI outperforms geo-statistical inversion is at the position of the small well at the upper right corner in (Fig.5b). Well information from this well was not provided to the geo-statistical inversion, and as a result, one can see in Figure (5a) that the VpVs ratio from statistical inversion does not follow the well-log result at the location of this well. However, the VpVs ratio from elastic FWI follows well-log closely within the limits of its bandwidth.

As a further assessment of the FWI result we show the initial image depth slice, migrated using initial Vp model overlaid with the initial VpVs ratio in Figure (6a). Again, all the structures recovered here are recovered directly from the seismic, since the initial Vs model was simply the initial Vp model scaled by a constant. The same overlay but using the final image and the final VpVs ratio from the elastic FWI is shown in Figure (6b). We are pleased to see that the channel is well captured in the VpVs ratio result. Most other structures also correlate well with the inverted VpVs ratio. There is an abundance of extra interpretable information centered around the prospect area that are unseen by conventional seismic but are revealed from information inverted by elastic FWI.

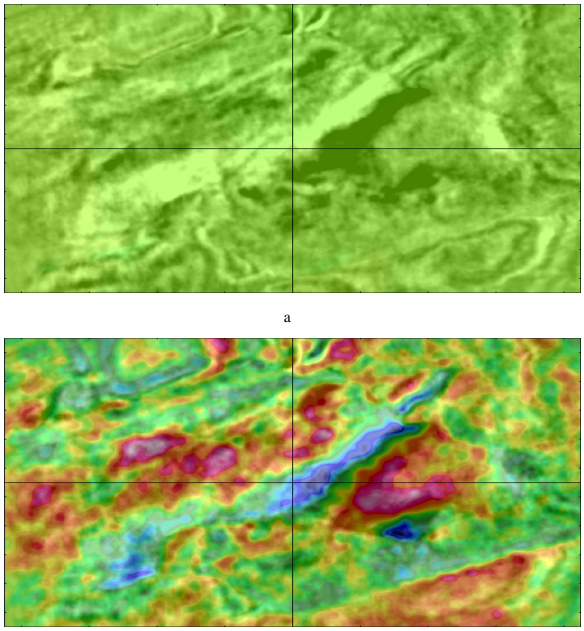

a

b

Figure 6: (a) Overlaid seismic with VpVs ratio for the initial model. (b) Overlaid seismic with the output VpVs ratio from elastic FWI.

CONCLUSION

We have developed a method of elastic FWI using a Vp−Vs−density parametrization, and applied it to an area where pre-existing standard geo-statistical AVO inversion results using well-constraints were available for comparison. The FWI used here did not use any prior well-log information. Our recovery of Vp, density, and VpVs ratio suggest that such an inversion can be relatively robust, and the results obtained in general compare quite favorably to standard geo-statistical results, and appear to outperform it in the recovery of density. This suggests that despite the computational cost, elastic FWI may be an effective tool for elastic parameter recovery in exploration or step-out settings, where limited well-log information is available. In addition, elastic FWI may be used to not only reconstruct elastic properties, but may also provide additional parameter volumes that can be used in the interpretation and identification of hydrocarbon reservoirs.

ACKNOWLEDGMENTS

We thank John Washbourne and Chris Manuel for the dedicated time for this work. Ashley Ezzy provided critical analysis. Reynaldo Cardona oversaw the execution of the project. Lin Zhang and Mark Fan provided the leadership and the steering. We thank Vickie Foster for coordinating the internal review, and Justin Tan, Xiang Xiao for the reviewing of the manuscript. The authors would like to thank Geoscience Australia for providing access to various data available in the public domain and Chevron Australia for coordination of various data types for provision of the processed OBN data. We thank Chevron Corporation for the permission to publish this work.